IEEE Access
Multidisciplinary | Rapid Review | Open Access Journal

Received November 12, 2020, accepted November 27, 2020, date of publication December 7, 2020,
date of current version December 28, 2020.

Digital Object Identifier 10.1109/ACCESS.2020.3042983

A Calculation Method to Adjust the Short-Circuit Impedance of a Transformer

ZHIJUN YE[1], WANG YU[1], JULONG GOU[1], KAIJIA TAN[1], WENHUI ZENG[2], BONAN AN[3], (Student Member, IEEE), AND YONG LI[3], (Senior Member, IEEE)

[1]College of Information Science and Engineering, Huaqiao University, Xiamen 361021, China
[2]State Grid Quanzhou Power Supply Company, Quanzhou 362000, China
[3]College of Electrical and Information Engineering, Hunan University, Changsha 410082, China

Corresponding author: Wang Yu (517662697@ qq.com)

This work was supported in part by the Education and Scientific Research Project for Middle-Aged and Young Teachers in Fujian Province under Grant JAT160023; in part by the 111 Project of China under Grant B17016; and in part by the Subsidized Project for Postgraduates' Innovative Fund in Scientific Research of Huaqiao University.

ABSTRACT A staggered transformer of power frequency inverters in uninterruptible power supplies (UPS) can be used as both a voltage transformer and an inductance of filter circuits to replace a traditional reactor. In this paper, a method is presented to calculate the short-circuit impedance Z_k of a staggered transformer. which can be adjusted by using different arrangements of primary and secondary windings. Using the structure parameters of core and winding and the magnetic circuit analysis method, the proposed method in this paper can accurately calculate Z_k. This high-precision and simple formula is easy to apply in engineering. First, a model of the single-phase isolation transformer (the winding arrangement is PSSPPS) is established using FLUX 3D and verified by comparing the simulated data with the measured data. Second, short-circuit impedances of four typical winding arrangements (PSSPPS, SPSPPS, PSPSPS, PPPSSS) are obtained by simulation. The results show that the errors between the simulation and calculation are less than 10%, which proves the validity of the method. Finally, an analysis of the magnetic field parameters of the staggered transformers with different winding structures shows that the number of parallel branches of leakage flux magnetic circuits increases with the complexity of the winding structure, which is consistent with the theory.

INDEX TERMS Staggered transformer, finite element method, short-circuit impedance, flux path.

I. INTRODUCTION

Power transformer is one of the important equipment in the power grid [1], [2]. Short-circuit impedance Z_k is a major parameter of the transformer and should not be ignored in transformer design, manufacture, and operation [3], [4]. By improving Z_k, the transformer can change the voltage in uninterruptible power supplies (UPS) and act as an inductance filter to save space and cost [5]. The distribution and size of the leakage magnetic field change with the winding structure of the transformer, which adjust Z_k [6]. Hence, studying the effect of the winding arrangement on Z_k is of great practical significance for reducing the cost and improving the performance of transformers.

The value of Z_k affects the electromagnetic force of the transformer and the voltage fluctuation of the power grid [7].

The associate editor coordinating the review of this manuscript and approving it for publication was Su Yan.

For a wide range of transformers, the calculation methods for Z_k include the magnetic circuit method, magnetic field energy method [8], magnetic leakage method, analytical method and field circuit coupling method [9]–[11]. In [12], a combination of the power method and average geometric distance method was proposed to calculate the short-circuit impedance of transformers. This combined method was characterized by the simplicity of its formula, a low number of limitation conditions and a high level of precision. In [13], the change in leakage inductance L_k in single-phase power transformers when a fault occurs in the grid was described, and the winding deformation caused by the current stress was considered. However, an overlarge winding current more likely causes serious saturation of the core. Thus, the use of linear ferromagnetic materials may cause some deviation in the conclusion. In [14], a method to calculate Z_k was proposed based on the principle that the magnetic force line was produced by the effective conductor in the winding.

The finite element method (FEM) can flexibly handle nonlinear and complex problems. In particular, the method adopts the matrix expression, which is convenient to program and fits the electromagnetic field expression. A finite element model of single-phase transformers was established in [15] using Flux software. The effect of saturation in the transformer core on Z_k during a sudden short-circuit of the transformer was studied, but the leakage magnetic field of the winding was not analysed in-depth. Leakage reactance of a 9-winding 3-phase 3-column transformer based on FEM was calculated in [16], and a change in leakage reactance calculated in the steady state and transient state was observed due to different winding structure arrangements. The calculation and measured results were compared, but the effect of core saturation was ignored.

In this paper, a method is presented to calculate the Z_k of the axially directed multi-segment windings transformer using the structural parameters of transformers. First, the relationship between Z_k and the winding distribution is deduced based on a magnetic circuit analysis. Second, using the FEM software FLUX 3D, the simulation model of the staggered transformer with a rated capacity of 20 kVA, a primary voltage of 104 V and a secondary voltage of 240 V is established using the magnetic circuit coupling method. The accuracy of the model is verified by measurement data. Third, the transformer with different winding arrangements is simulated and analysed, the short-circuit impedance of the transformer is obtained, and the accuracy of the theory is verified by comparing the simulated and calculated values. Finally, the magnetic field parameters of staggered transformers with different winding structures are analysed.

II. RELATION BETWEEN THE SHORT-CIRCUIT IMPEDANCE AND WINDING DISTRIBUTION

The Z_k of transformers is composed of short-circuit resistance R_k and short-circuit impedance X_k. R_k is related to the characteristics of the winding; when the effect of temperature is ignored, the value of R_k remains unchanged [17]. X_k can be adjusted by different winding arrangements [18]; according to the definition of X_k, we observe the following:

$$X_k = 2\pi f L_k = 2\pi f \frac{\Psi_\sigma}{I} = 2\pi f \frac{N\Phi_\sigma}{I} \tag{1}$$

f is the frequency of the power supply, Ψ_σ is the flux leakage chain, N is the number of winding turns, and Φ_σ is the flux leakage. Therefore, when N and the short-circuit current I are constant, L_k is proportional to Φ_σ.

From the law of magnetic circuit and the theory of magnetic reluctance and electromagnetism [19], we can conclude the following:

$$\Phi_\sigma = \frac{F}{R_\sigma} \tag{2}$$

$$F = NI \tag{3}$$

$$R_\sigma = \frac{l}{\mu S} \tag{4}$$

F is the leakage magnetic potential; R_σ, l, μ and S are the leakage magnetic reluctance, length, permeability and cross-sectional area of the closed magnetic circuit formed by the leakage flux, respectively. After substituting Eqs. (2), (3) and (4) into Eq. (1) and converting the parameters of the secondary side to those of the primary side, L_k can be expressed as follows:

$$L_k = \frac{N_P^2}{\left(R_{\sigma P} + \frac{R_{\sigma S}}{k^2}\right)} \tag{5}$$

k is the transformer ratio; $k = N_P/N_S$; N_P is the number of primary winding turns; and N_S is the number of secondary winding turns. According to Eq. (5), the calculation of L_k is ultimately attributed to the calculation of the leakage magnetic reluctance of the primary $R_{\sigma P}$ and secondary winding $R_{\sigma S}$. Because the permeability of the core μ_{Fe} is much greater than that of the air μ_{air}, the leakage magnetic reluctance inside the core can be ignored. From Eq. (4), R_σ can be calculated by the structural parameters of the transformer to L_k and Z_k of the transformer.

The structure of transformer winding is divided into three types: layer, pie, and staggered [3]. In this paper, the winding of the single-phase isolation transformer adopts a staggered structure, and the winding on the same side adopts a parallel connection. The winding is symmetrically distributed on both sides of the core: the primary side is the low-voltage side, and the secondary side is the high-voltage side.

The simplified schematic diagram of the two windings is shown in Fig. 1. The magnetic flux of the transformer consists of the main flux Φ and Φ_σ, where the latter serves as the magnetic flux of primary winding P or secondary winding S in the separate turn-chain. To more intuitively express the leakage flux loop, the leakage flux region of the primary and secondary windings are divided. In the calculation, the leakage flux of the secondary winding can be converted to the primary side, and the total flux linkage and total reactance produced can be calculated [5].

According to the corresponding relationship between magnetic circuit and electric circuit, the leakage flux magnetic circuit of region A of the primary winding in Fig. 1 (a) is shown in Fig. 2.

Fig. 1 shows that the structure of leakage flux area A of the primary winding of the PSSP structure is identical to that of area C. Therefore, according to the circuit principle, the leakage flux of the primary winding $\Phi_{\sigma P}$ in Fig. 2 can be expressed as follows [20]:

$$\Phi_{\sigma P} = N_P I_P \frac{8R_1 + 4R_2}{R_1 R_2} \tag{6}$$

R_1 and R_2 are the leakage magnetic reluctance of the leakage flux closed loop $\Phi_{\sigma p11}$, $\Phi_{\sigma p12}$, $\Phi_{\sigma p21}$ and $\Phi_{\sigma p22}$ in air.

In Fig. 1 (a), the leakage flux magnetic circuit of area B of the secondary winding is shown in Fig. 3.

The leakage flux of the secondary winding $\Phi_{\sigma S}$ can be expressed as follows:

$$\Phi_{\sigma S} = N_S I_S \frac{2R_2R_3 + 8R_2R_4 + 8R_3R_4}{R_2R_3R_4} \tag{7}$$

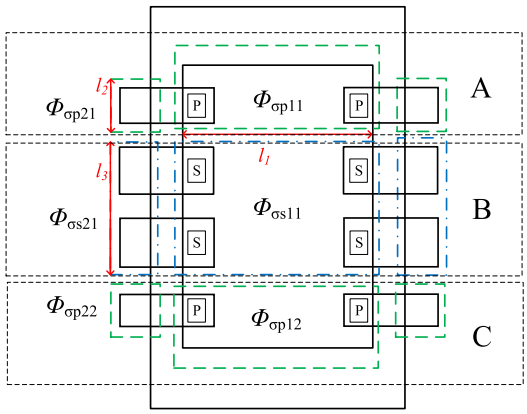

(a) Winding Distribution of PSSP

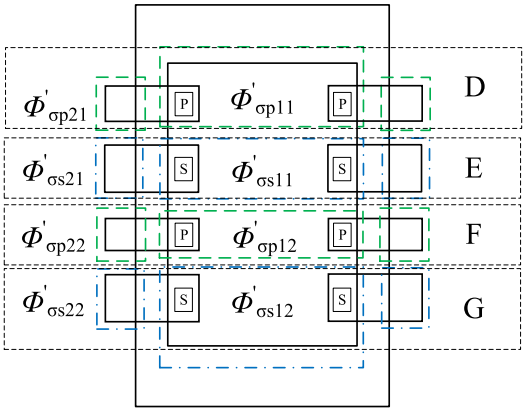

(b) Winding Distribution of PSPS

FIGURE 1. Schematic diagram of the distribution of different windings.

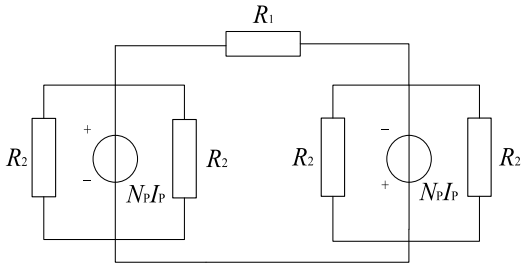

FIGURE 2. Primary-winding magnetic circuit diagram of the PSSP structure.

R_3 and R_4 are the leakage magnetic reluctances of the leakage flux closed loop $\Phi_{\sigma s21}$ and $\Phi_{\sigma s11}$ in air, respectively. By substituting Eqs. (6) and (7) into Eq. (5), we can obtain the L_k of the PSSP structure.

$$L_k = N_P^2 \left(\frac{8R_1 + 4R_2}{R_1R_2} + k^2 \frac{2R_2R_3 + 8R_2R_4 + 8R_3R_4}{R_2R_3R_4} \right) \tag{8}$$

According to Eq. (4), R_σ is directly proportional to l and inversely proportional to S, so $R_3 \approx 2R_2$ and $R_4 \approx 2R_1$. Therefore, Eq. (8) can be simplified as follows:

$$L_k = N_P^2 \left(\frac{8R_1 + 4R_2}{R_1R_2} + k^2 \frac{12R_1 + R_2}{R_1R_2} \right) \tag{9}$$

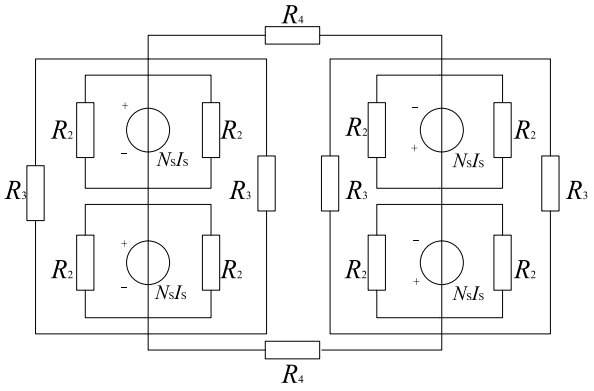

FIGURE 3. Secondary-winding magnetic circuit diagram of the PSSP structure.

Similarly, the primary and secondary winding structures in Fig. 1 (b) are identical. Using the magnetic circuit analysis method, we can obtain the L'_k of the PSPS structure:

$$L'_k = N_P^2 \left(\frac{8R_1 + 3R_2}{R_1R_2} + k^2 \frac{8R_1 + 3R_2}{R_1R_2} \right) \tag{10}$$

Compared with Eqs. (9) and (10), u (R_1, R_2, k) is defined as the difference in leakage magnetic reluctance in the corresponding formula:

$$u(R_1, R_2, k) = \frac{R_2}{R_1R_2} + k^2 \frac{4\,R_1 - 2\,R_2}{R_1R_2} \tag{11}$$

In Eq. (11), the numerical ranges of the parameters are as follows: $0 < R_1 < +\infty$, $0 < R_2 < +\infty$, and $0 < k < 1$. The graph of u (R_1, R_2, k) for these three parameters is drawn by MATLAB. To better represent their relationship, the graph with the maximum values of R_1 and R_2 of 100 Ω is intercepted, as shown in Fig. 4.

Fig. 4 shows that u (R_1, R_2, k) is always greater than zero, so the following conclusion can be drawn:

$$L_k > L'_k \tag{12}$$

In conclusion, the R_σ of the transformer can be effectively changed by altering the arrangement of primary and secondary winding. Different winding arrangements do not change R_k, according to the definition of Z_k [4]; the short-circuit impedance relationship of these two winding connection modes can be expressed as follows:

$$Z_k > Z'_k \tag{13}$$

Thus, when the primary- and secondary-side structures of the staggered winding become increasingly complex, the number of parallel leakage reluctances in the magnetic circuit will increase; from the perspective of magnetic circuit analysis, the total leakage reluctance will decrease. Because the relationship between leakage impedance and leakage reluctance is that they are opposite, the leakage reluctance will increase with the complexity of the winding structure.

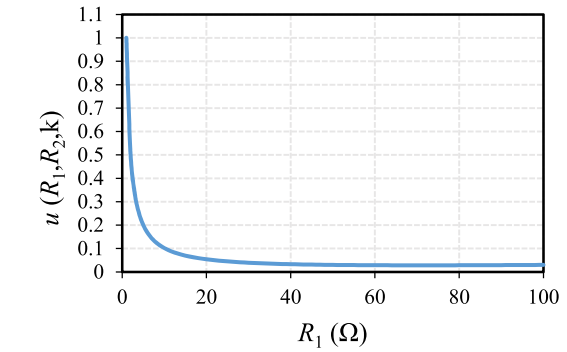

(a) Graph of R_1

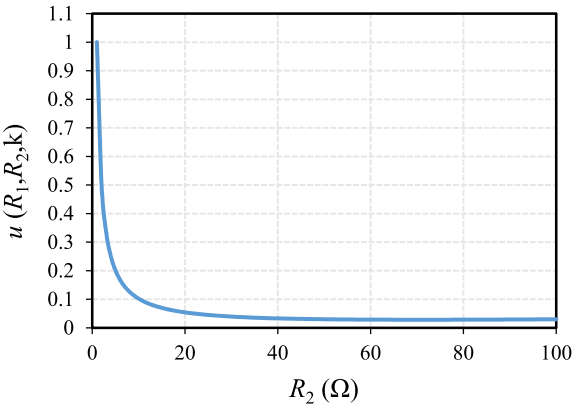

(b) Graph of R_2

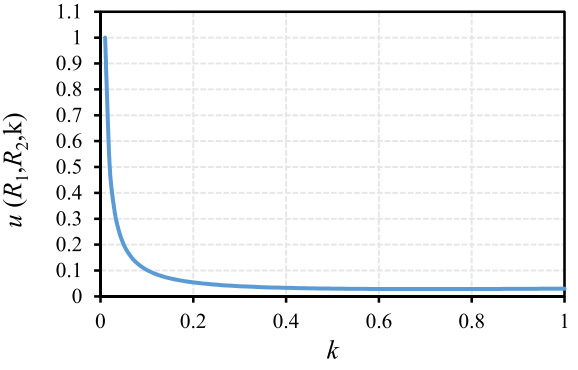

(c) Graph of k

FIGURE 4. Graph of u (R_1, R_2, k) selected for different parameters.

III. MODELLING OF THE SINGLE-PHASE TRANSFORMER

A. MODEL PARAMETER

A single-phase staggered transformer model was constructed with the FEM software FLUX 3D. Its accuracy was verified by the comparison between the measured and simulated data. The experimental test platform is presented in Fig. 5, which consists of the transformer, load bank, oscilloscope, air switch, analyser, and three-phase power.

To accurately establish the finite element model of the transformer, the electrical parameters related to the single-phase transformer are shown in Table 1, including the rated power, the voltage and current of the primary winding, and the percentage of short-circuit voltage.

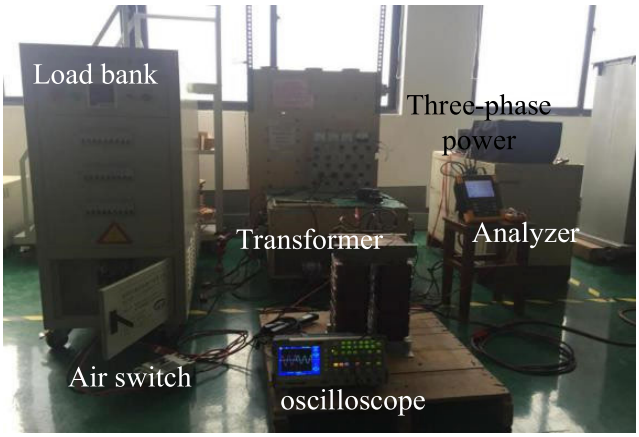

FIGURE 5. Experimental test platform.

TABLE 1. Electrical parameters of the transformer.

Parameter	Value	Parameter	Value
Rated power P_N (kW)	14	Rated frequency f_N (Hz)	50
Primary rated voltage U_{1N}(V)	104	Secondary rated voltage U_{2N}(V)	240
Primary rated current I_{1N}(A)	134.6	Secondary rated current I_{2N}(A)	58.3
Percentage of short-circuit voltage	6%	Percentage of no-load current	4%

The structural parameters related to the single-phase transformer are shown in Table 2. When calculating Z_k, we should pay special attention to these parameters: the length of core window l_1; the average distance between the winding and core δ; the height of winding l_2; the distance between the winding packages on the same side h; and the number of turns of primary winding N_P and secondary winding N_S.

The simulation model was established in Flux 3D based on the geometric parameters measured by the transformer, where P and S are the primary and secondary windings, respectively. The B-H curve of the core material is shown in Fig. 6.

To save model computation time and storage space, only half the model of the transformer was built, and one key automatic segmentation function was used. The adaptive mesh generation method was used for the model, and the mesh number was 147278. Flux 3D uses the Newton-Raphson method to solve the nonlinear system; its accuracy threshold is set as 1.0E-4, and the maximum number of iterations is 100. The boundary conditions are described by two parallel and superimposed hexahedrons, the surfaces of the outer parallelepiped are the image of the infinite body, where the potential and field are equal to zero. The segmentation network of the generated model is shown in Fig. 7.

TABLE 2. Structural parameters of the transformer.

Parameter	Value	Parameter	Value
Length of core l_{FE}(mm)	210	Height of core h_{FE}(mm)	417
Length of core window l_1(mm)	68	Height of core window h_1(mm)	275
Height of winding l_2(mm)	41	Average distance between winding and core δ(mm)	6
Number of packages in the same side winding	6	Distance between winding packages on the same side h(mm)	5
Core thickness D(mm)	127	Winding thickness d(mm)	20
Turns of primary winding N_P	42	Turns of secondary winding N_S	97

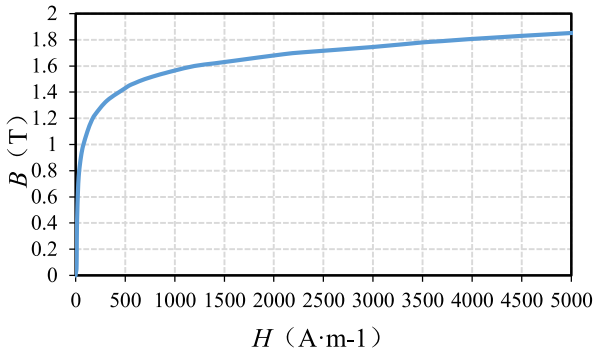

FIGURE 6. B-H curve of the core material.

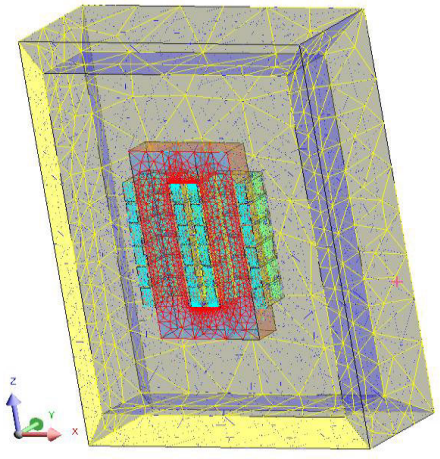

FIGURE 7. Half-model subdivision diagram of the transformer.

The coupling circuit of the transformer model is shown in Fig. 8. The input of the transformer was simplified

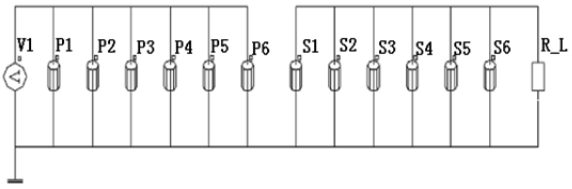

FIGURE 8. Steady-state coupled circuit.

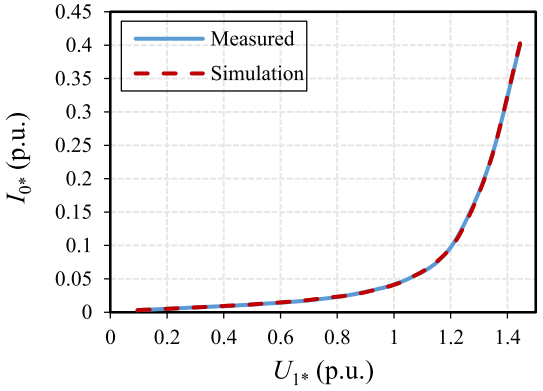

FIGURE 9. No-load characteristic curve.

to the primary-side voltage source $V1$. $P1$–$P6$ and $S1$–$S6$ connected in parallel are the coupling elements of the primary and secondary windings of the circuit, respectively. R_L is the secondary-side load. By setting its resistance value, we obtained the simulated data under various working conditions. When $R\_L=10^8\Omega$, the transformer was in no-load running. When $R\_L=U_{2N}/I_{2N}$, the transformer ran at the rated load. In the short circuit, R_L was set as $10^{-8}\Omega$, and the secondary side was connected to voltage source $V2$.

B. MODEL VALIDATION

The model verification of the transformer was divided into two parts:

(a) Steady-state verification: no-load test, short-circuit test and rated-load test.

(b) Transient verification: load sudden short-circuit test.

1) NO-LOAD TEST

During the no-load simulation experiment, the primary side of the transformer was connected to a power supply. The voltage was 0-1.5U_{1N}. The no-load characteristic curve $I_{0*} = f(U_{1*})$ was obtained as shown in Fig. 9.

In Fig. 9, the simulated values almost coincided with the measured values, and the error was less than 3%. When the voltage was 0-U_{1*}, the core was unsaturated, and a positively linear relationship was found between the no-load current and voltage. When the voltage reached the rated value, the error between the simulated and measured data of the no-load current was 1.77%. When the voltage further increased, the no-load current sharply increased as the core gradually entered the depth saturation.

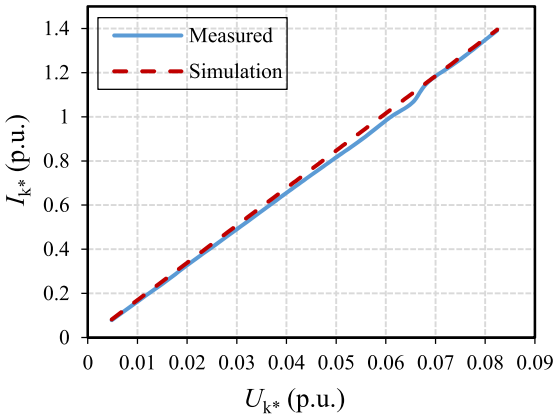

FIGURE 10. Short-circuit characteristic curve.

TABLE 3. Rated load test.

Parameter	I_1 (A)	U_2 (V)	I_2 (A)
Measured data	138	235.1	58.02
Simulated data	132.63	232.13	57.29
Error	3.89%	1.26%	1.26%

2) SHORT-CIRCUIT TEST

In this test, the low-voltage side of the transformer was short-circuited, and the high-voltage side was connected to the input voltage source. The amplitude of the short-circuit current increased with the growing input voltage. The short-circuit characteristic curve $I_{k*} = f(U_{k*})$ is shown in Fig. 10.

As shown in Fig. 10, U_{k*} and I_{k*} are the short-circuit voltage and current of the transformer, respectively, which have a linear relationship. Under the rated current, the error between the short-circuit voltage simulated and measured data was 3.61%.

3) RATED-LOAD TEST

Under rated-load operation, the input voltage U_1 of the primary side was 104 V, and the secondary side was connected to the pure resistance load. The corresponding relationship of parameters is shown in Table 3.

In Table 3, the error between the simulated and measured data of the voltage and current during rated-load operation was within 4%.

4) TRANSIENT SHORT-CIRCUIT TEST

In this test, the load side was connected with a resistance R_L and a switch in parallel. When the switch was suddenly closed, the load was short-circuited.

The coupling circuit of the transient short-circuit running experiment is shown in Fig. 11.

Unlike the steady-state operation test, the transient short-circuit operation test had a switch in the coupling circuit

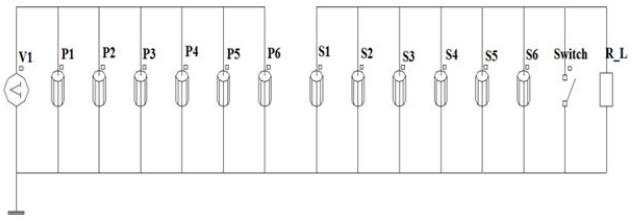

FIGURE 11. Transient short-circuit experiment coupled circuit.

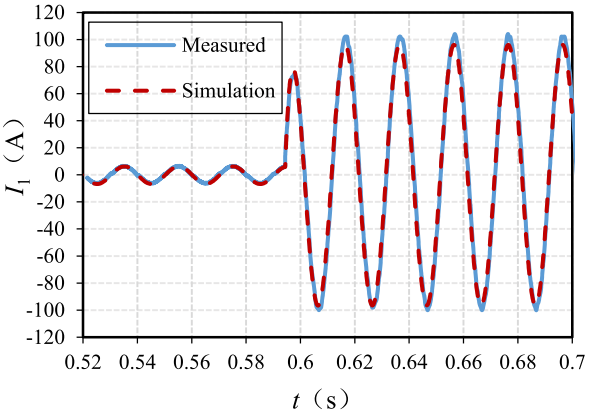

FIGURE 12. Change in the primary-side current with time.

diagram. The closing time and internal resistance value of the switch could be set.

According to the short-circuit time measured by the field transient short-circuit test, the simulation software was set to be simultaneously subject to the short-circuit by closing the switch when $t = 0.5944$ s. Then, the curve of the measured and simulated values of the primary-side current with time was obtained, as shown in Fig. 12.

The simulation results indicate that the primary-side current is at a maximum when $t = 0.6064$ s, and the error between simulated and measured data is 3.4%. In conclusion, the comparison between the simulated and measured data of the transformer demonstrates that the errors of all operating experiments are less than 5%, which is within the allowable range of engineering. This result verifies the accuracy of the simulation model. Thus, the model can be used to further study the effect of the winding arrangement sequence on Z_k of transformers.

The Z_k of the transformer can be obtained from the short-circuit test of the transformer [4]. Its equivalent circuit diagram is shown in Fig. 13.

R_1 and R_2' are measured by the short-circuit test. Therefore, the values of R_1 and R_2' in Fig. 12(c) are based on the measured data. Table 4 can be obtained by comparing the data of the three equivalent circuit diagrams.

In Table 4, all comparison errors of simulated data, calculated values and measured values are within 5% when R and X_σ are equivalent to the primary side. The calculated values X_σ in Table 4 are obtained from the design parameters of the transformer.

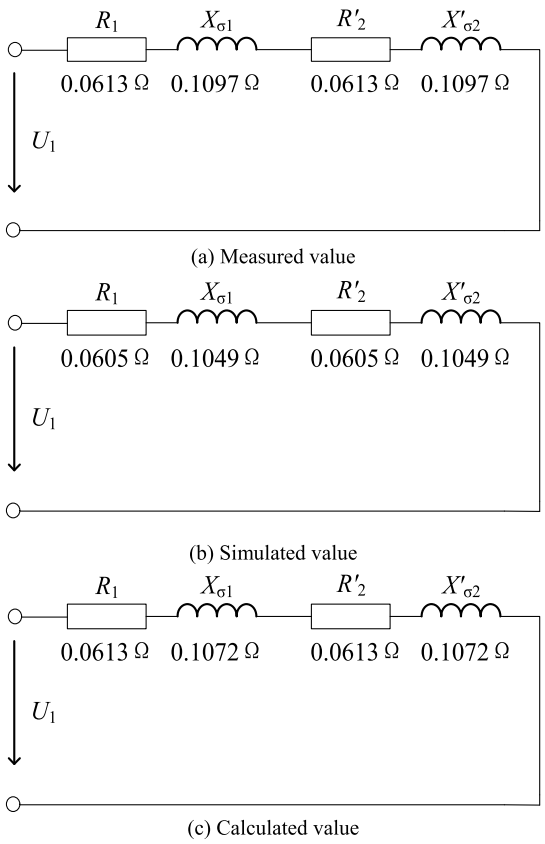

FIGURE 13. Equivalent circuit diagram of the transformer short circuit.

TABLE 4. Short-circuit test.

Parameter	$X_\sigma(\Omega)$	$\triangle X_\sigma(\%)$	$Z_k(\Omega)$	$\triangle Z_k(\%)$
Measured data	0.2194	Reference	0.2513	Reference
Simulated data	0.2098	-3.85	0.2422	-3.62
Calculated data	0.2144	-2.28	0.2470	-1.71

IV. EFFECT OF THE WINDING ARRANGEMENT ON THE SHORT-CIRCUIT IMPEDANCE

A. ILLUSTRATIVE EXAMPLES

The PSSPPS staggered arrangement with symmetrical structure on the left and right was adopted in the original transformer winding. Theoretically, there are 20 different winding permutations and combinations. Considering the structure symmetry, two air gaps in the transformer iron yoke and other factors, four types of typical winding arrangements are listed as follows, including the initial transformer PSSPPS structure, and the SPSPPS, PSPSPS, PPPSSS structures after the change in winding arrangement, as shown in Fig. 14.

According to the theoretical derivation in the second section, with the winding structure of PSSPPS as an example, the primary leakage flux magnetic circuit is composed of two parts in Fig. 15.

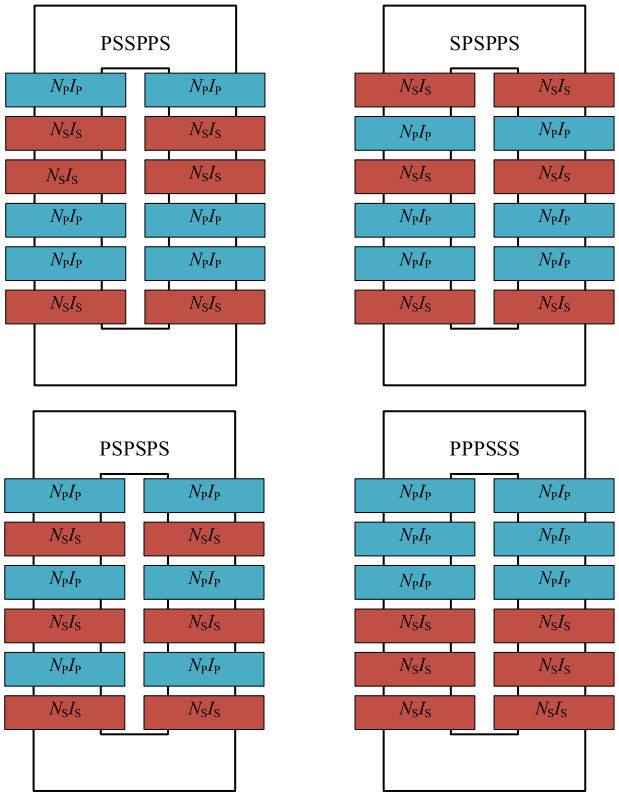

FIGURE 14. Winding arrangement sequence diagram.

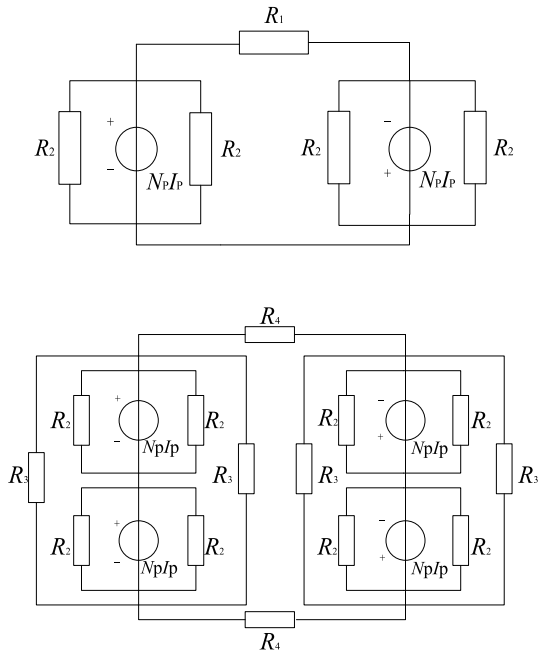

FIGURE 15. Primary-side leakage flux magnetic circuit diagram of the transformer with the PSSPPS structure.

According to Eq. (5), the short-circuit inductance of the primary-side L_{kP} of the transformer can be obtained as follows:

$$L_{kP} = N_P^2 \frac{8R_1R_2R_3 + 12R_1R_2R_4 + 2R_1R_3R_4 + 2R_2R_3R_4}{R_1R_2R_3R_4} \tag{14}$$

TABLE 5. Calculation parameters of the short-circuit inductance.

Parameter	Value
R_1	l_1=68 mm S_1=7339 mm^2
R_2	L_2=41 mm S_2=2864 mm^2
R_3	L_3=87 mm S_3=2864 mm^2
R_4	L_4=68 mm S_4=15537 mm^2
N_P	42
k	42/97

TABLE 6. Short-circuit impedance of different winding arrangements.

Winding arrangement	PSSPPS	SPSPPS	PSPSPS	PPPSSS
U_k(V)	14.6	14.6	14.6	14.6
Simulated data $Z_k(\Omega)$	0.2422	0.2032	0.1742	0.8602
Calculated data $Z_k(\Omega)$	0.2305	0.1982	0.1858	0.8224
Error	-4.83%	-2.46%	6.66%	-4.39%
Adjustment Rate of Z_k	Reference Value	-14.01%	-19.39%	256.79%

The selection of parameters in Eq. (14) is shown in Table 5. In Table 5, the magnetic circuit length and cross-section area of the leakage magnetic reluctance are selected from Table 2.

Fig. 14 shows that the structure of primary and secondary windings of PSSPPS is symmetrical, so the calculation method of the leakage magnetic resistance of the secondary side is consistent with that of the primary side. Therefore, let $R = (8R_1R_2R_3 + 12R_1R_2R_4 + 2R_1R_3R_4)/R_1R_2R_3R_4$ and convert the leakage magnetic reluctance of the secondary side to the that of the primary side; then, the L_k of the transformer is as follows:

$$L_k = N_P^2(R + k^2R) \tag{15}$$

Neglecting the change of winding with temperature, R_k is subject to the measured data. Using the values in Table 4, the Z_k of the transformer with the PSSPPS winding structure is 0.2305Ω. The Z_k values of the four different winding structures are shown in Table 6.

According to the data in Table 6, comparison errors between calculated and simulated values are less than 10%, which verifies the correctness of the calculation method in this paper. Compared with the initial transformer (PSSPPS), PPPSSS has the largest Z_k, PSPSPS has the smallest Z_k, and the other values are in between. The results are consistent with the theoretical derivation.

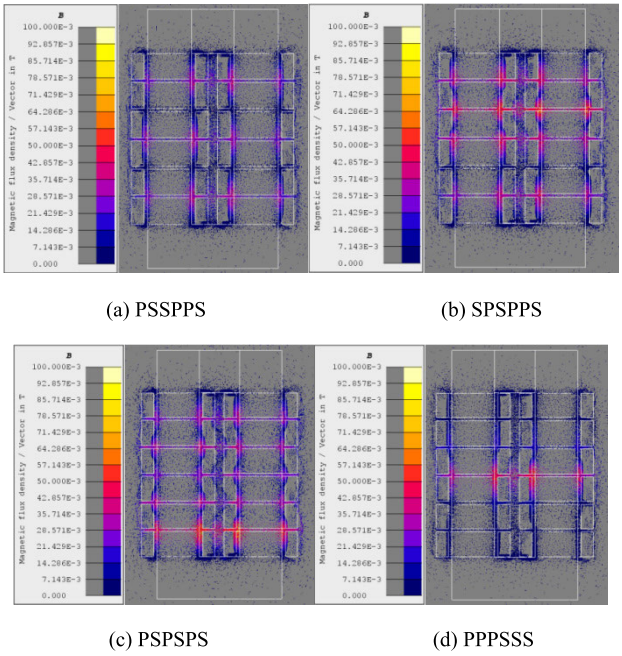

(a) PSSPPS (b) SPSPPS

(c) PSPSPS (d) PPPSSS

FIGURE 16. Distribution of the magnetic flux density with different winding arrangements.

B. MAGNETIC FIELD ANALYSIS OF THE TRANSFORMER CORE

Fig. 16 shows the flux density diagram under different winding distributions. Flux density B slightly changes with different winding distributions, but the distribution of B changes greatly. From the magnetic field principle of the transformer, we can conclude that a magnetic circuit will be formed between the high and low voltage windings. Taking the distribution of PSSPPS windings in Fig. 16 (a) as an example, there are three adjacent high and low voltage windings (PS or SP), which will produce three magnetic circuit channels between the windings. According to Eq. (4), under the condition of constant permeability μ and cross-sectional area S, R_σ is directly proportional to l; a larger magnetic resistance corresponds to a smaller leakage flux, a smaller leakage reactance and a greater short-circuit current.

Fig. 16 shows that there are four magnetic circuits between the windings with the SPSPPS distribution, five magnetic circuits between the windings with the PSPSPS distribution, and one magnetic circuit between the windings with the PPPSSS distribution. Therefore, the maximum short-circuit current distributed by PSPSPS in the winding is the largest, while the maximum short-circuit current in the PPPSSS distribution of the winding is the smallest. The maximum short-circuit current of the SPSPPS distribution and the PSSPPS distribution is between these two values. The analysis results are consistent with the theoretical calculation.

Fig. 17 shows the relative magnetic permeability distribution when the short-circuit current was at a maximum in different winding arrangements.

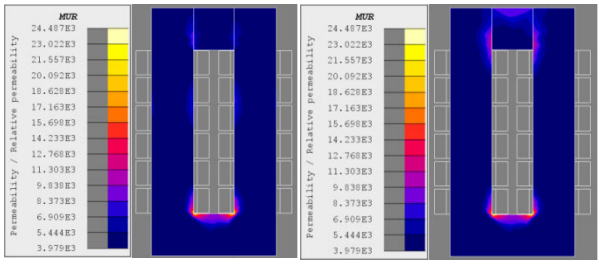

(a) PSSPPS (b) SPSPPS

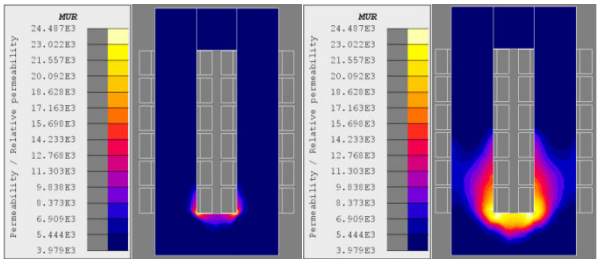

(c) PSPSPS (d) PPPSSS

FIGURE 17. Distribution of the relative magnetic permeability of the core with different winding arrangements and maximum short-circuit current.

Fig. 17 shows the following:

(a) In different winding arrangements, when the short-circuit current was maximum, the relative permeability in the transformer core was above 3979, which is much higher than 1. Thus, the transformer core was far from the saturated state.

(b) As shown in Fig. 17 (a), the maximum relative magnetic permeability was located at the inner angle of the transformer and lower iron yoke. There were two reasons for this: first, the magnetic circuit passing through the inner angle of the transformer core was relatively short, resulting in the lowest magnetic energy consumption. Second, the inner angle of the upper iron yoke was connected to the core air gap. Under the effect of the air gap, the magnetic resistance increased with a small magnetic path distribution and magnetic permeability. Therefore, the relative magnetic permeability at the inner angle of the lower iron yoke was larger than that at the upper iron yoke.

(c) The relative magnetic permeability mutated at the air gap of the transformer because it was much lower than that at the surrounding iron core due to the much larger magnetic resistance of the air gap than that of ferromagnetic materials.

(d) When the winding distribution was changed, the intensity and path of leakage flux distribution varied, and the relative magnetic conductivity distribution at the core of transformer experienced a large change.

C. ANALYSIS OF THE MAGNETIC CIRCUIT ANGLE

The magnetic field intensity distribution when the short-circuit current was maximum under different winding arrangements is presented in Fig. 18.

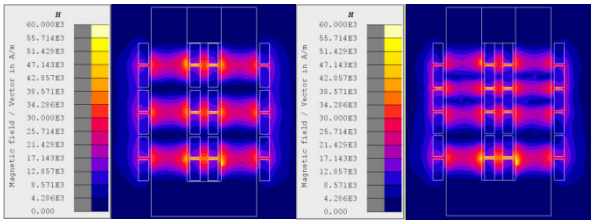

(a) PSSPPS (b) SPSPPS

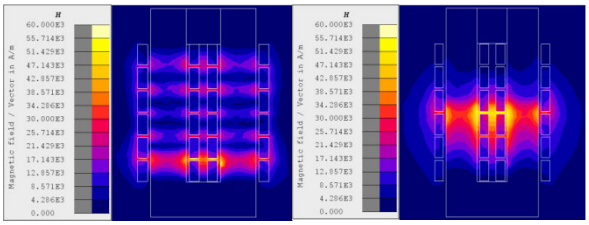

(c) PSPSPS (d) PPPSSS

FIGURE 18. Distribution of the magnetic field intensity of the core with different winding arrangements and maximum short-circuit current.

The initial transformer in Fig. 18 shows the following:

(a) The magnetic field was symmetrically distributed because of the symmetrical distribution of windings on the two core columns.

(b) A magnetic circuit was formed between any set of connected "PS" or "SP" windings.

(c) The magnetic field intensity of the air gap between identical grade windings (PP or SS) was almost zero since the magnetic flux paths had identical sizes and opposite directions.

(d) The distribution of magnetic field intensities varied with different arrangements of the substance windings.

(e) The magnetic circuit varied in different winding arrangements. The transformer formed 3, 4, 5, and 1 magnetic path between PS, SP and PS in Fig. 18(a), Fig. 18(b), Fig. 18(c), Fig. 18(d), respectively.

(f) With an increase in the number of magnetic leakage flux paths, the maximum magnetic field intensity of the transformer decreased. With less leakage magnetic circuit, more leakage magnetic field passed through the magnetic circuit. As a result, the magnetic field was at a maximum when there was only one magnetic path in the PPPSSS, as shown in Fig. 18(d).

Based on the comparison of the short-circuit impedances of different winding arrangements in Table 4, when the short-circuit current is at a maximum, the short-circuit impedance increases with the decrease in magnetic leakage flux paths.

V. CONCLUSION

This paper presents a method for calculating the short-circuit impedance of the axially directed multi-segment windings transformer, and the magnetic field parameters of transformers with different winding structures are compared and analysed. The conclusions are as follows:

(1) Based on the magnetic circuit analysis method, the short-circuit impedance of the axially directed multi-segment windings transformer can be calculated by the structural parameters of the transformer core and winding. The leakage magnetic reluctance on the same side of the core column is parallel structure. Since the leakage flux magnetic circuit in the core window is excited by the magnetic potential on both sides, the leakage magnetic reluctance in the window is in series.

(2) Changing the arrangement of transformer windings will affect the change in the magnetic circuit and alter the leakage magnetic field distribution and short-circuit impedance. In the four different winding structures studied, short-circuit currents reached the maximum relative permeability at the inner angle of the core and the minimum value at the outer angle of the core. A less magnetic circuit has a stronger magnetic field. The magnetic flux leakage path varies under different winding arrangements. Compared to the original transformer winding, the increase in magnetic circuit reduces the short-circuit impedance.

REFERENCES

[1] R. A. Abd El-Aal, K. Helal, A. M. M. Hassan, and S. S. Dessouky, "Prediction of transformers conditions and lifetime using furan compounds analysis," *IEEE Access*, vol. 7, pp. 102264–102273, 2019.

[2] J. Zhao, S. E. Zirka, Y. I. Moroz, C. M. Arturi, R. A. Walling, N. Tleis, and O. L. Tarchutkin, "Topological transient models of three-phase, three-legged transformer," *IEEE Access*, vol. 7, pp. 102519–102529, 2019.

[3] K. N. Yi, *Principle of Transformer Design*, 5nd ed. Beijing, China: China Power Press, 2003, pp. 195–218.

[4] Z. B. Zhang, *Principle and Application of Transformer*, 2nd ed. Beijing, China: Chemical Industry Press, 2007, pp. 18–21.

[5] Z. A. Wang and J. J. Liu, *Power Electronic Technology*. Beijing, China: Machinery Industry Press, 2009, pp. 218–219.

[6] C. X. Wang, "Calculation of transformer short circuit impedance by power method and average geometric distance method," *Transformer*, vol. 50, no. 12, pp. 14–16, 2016.

[7] W. Zhang, W. D. Xu, and C. X. Wang, "General law of short circuit impedance," *Transformer*, vol. 50, no. 11, pp. 20–23, 2013.

[8] P. Cheng, E. K. Cheng, and Y. R. Sun, "Calculation of short circuit impedance of amorphous alloy transformer," *Transformer*, vol. 53, no. 12, pp. 15–18, 2016.

[9] S. S. Wang, Y. M. Li, and N. N. Guo, "Calculation of transformer short circuit impedance by 'magnetic circuit' coupling method," *High voltage Technol.*, vol. 32, no. 11, pp. 11–14, 2006.

[10] J. Z. Xu, X. X. Liang, and X. L. Yao, "Composite short circuit impedance and circulating current calculation of multi winding transformer based on equivalent single turn inductance matri," *J. Chin. Electr. Eng. Sci.*, vol. 31, no. 34, pp. 135–141, 2011.

[11] Y. Li, L. N. Li, and Y. T. Jin, "Calculation and analysis of leakage magnetic field and passing short circuit impedance of axial double split generator transformer," *High voltage Technol.*, vol. 40, no. 6, pp. 1623–1629, 2014.

[12] X. B. Ruo, Q. F. Cheng, and C. H. Kang, "Modelling and impedance parameter design of multi winding transformer based on combined field circuit coupling method," *J. Chin. Electr. Eng. Sci.*, vol. 29, no. 9, pp. 104–111, 2009.

[13] Z. Ye, C. Kreischer, and S. T. Kulig, "Analysis of transformer short circuit characteristics based on 3-D finite element method," in *Proc. IEEE Power Eng. Autom. Conf.*, , Wuhan, China, Sep. 2011, pp. 90–93.

[14] W. G. Hurley, D. J. Wilcox, and P. S. McNamara, "Calculation of short circuit impedance and leakage impedance in transformer windings," in *Proc. 22nd Annu. IEEE Power Electron. Spec. Conf.*, Cambridge, MA, USA, Jun. 1991, pp. 651–658.

[15] M. Bagheri, M. Naderi, T. Blackburn, and T. Phung, "Frequency response analysis and short-circuit impedance measurement in detection of winding deformation within power transformers," *IEEE Elect. Insul. Mag.*, vol. 29, no. 3, pp. 33–40, May 2013.

[16] H. Fukumoto, T. Furukawa, H. Itoh, and M. Ohchi, "Calculating leakage reactance of 9-winding transformer using time-dependent 3D FEM analysis," in *Proc. 41st Annu. Conf. IEEE Ind. Electron. Soc.*, Yokohama, Japan, Nov. 2015, pp. 4459–4464.

[17] M. Bagheri, S. Nezhivenko, B. T. Phung, and T. Blackburn, "Air core transformer winding disk deformation: A precise study on mutual inductance variation and its influence on frequency response spectrum," *IEEE Access*, vol. 6, pp. 7476–7488, 2018.

[18] R. Prieto, J. A. Cobos, O. Garcia, and J. Uceda, "Interleaving techniques in magnetic components," in *Proc. Appl. Power Electron. Conf.*, Atlanta, GA, USA, 1997, pp. 931–936.

[19] K. H. Zhao and X. M. Chen, *Electromagnetics*, 6nd ed. Beijing, China: Higher Education Press, 2011, pp. 423–426.

[20] Z. Wei, C. Qianhong, S. C. Wong, M. Tse, and C. Lingling, "Reluctance circuit and optimization of a novel contactless transformer," (in Chinese), *Trans. China Electrotech. Soc.*, vol. 30, no. 27, pp. 108–116, Sep. 2010.

ZHIJUN YE received the B.S. degree in applied electronics technology from the Guilin University of Electronic Technology, in 2000, and the M.S. and Ph.D. degrees in electrical and drive engineering from the Dortmund University of Technology, Germany, in 2013.

From 2008 to 2013, he was a Research Assistant with the College of Electrical Drives and Mechatronics, Dortmund University of Technology, Germany. Since 2013, he has taught at the College of Information Science and Engineering, Huaqiao University, China. In addition, his main research interests include power transformer fault diagnosis and design, high-frequency transformer research, synchronous and asynchronous motor fault diagnosis, and design and power system relay protection.

WANG YU received the bachelor's degree in automation from Beijing Forestry University, Beijing, China, in 2009. He is currently pursuing the master's degree in electrical engineering with the College of Electrical and Information Engineering, Huaqiao University, Xiamen, China. His research interests include the short-circuit impedance characteristics of power transformers, power transformer fault diagnosis and design, and power system relay protection.

JULONG GOU received the bachelor's degree in electrical engineering and automation from Huaqiao University in Xiamen, Fujian, China, in 2018. His research interests include electromagnetic field numerical analysis, internal fault diagnosis and the simulation of large generators, transformer design, and saturation characteristics.

KAIJIA TAN received the bachelor's degree from the College of Mechatronics and Control Engineering, Hubei Normal University, Huangshi, Hunan, China, in 2013 and 2017, respectively. He is currently pursuing the master's degree in electrical engineering with the College of Electrical and Information Engineering, Huaqiao University, Xiamen, China. His research fields include high-frequency transformers and power electronic transformers.

WENHUI ZENG received the B.S. degree in electrical engineering and automation, and the M.S. degree in electrical engineering from National Huaqiao University, China, in 2017. Since 2017, he has been working as a Substation Maintenance Engineer with the Quanzhou Power Supply Company of State Grid, focusing on the maintenance and research of electric primary equipment.

BONAN AN (Student Member, IEEE) was born in Shandong, China, in 1992. He received the B.Sc. degree in electrical engineering from Southwest Jiaotong University, Sichuan, China, in 2015. He is currently pursuing the Ph.D. degree with the College of Electrical and Information Engineering, Hunan University, Changsha, China. His research interest is new topology railway power conditioning systems and intelligent electrified railway system design and optimization.

YONG LI (Senior Member, IEEE) was born in Henan, China, in 1982. He received the B.Sc. and Ph.D. degrees from the College of Electrical and Information Engineering, Hunan University (HNU), Changsha, China, in 2004 and 2011, respectively, and the Ph.D. degree from TU Dortmund University, Dortmund, Germany, in 2012. Since 2009, he has been a Research Associate with the Institute of Energy Systems, Energy Efficiency, and Energy Economics, TU Dortmund University. Since 2012, he has been a Research Fellow with the University of Queensland, Australia. Since 2014, he has been a Full Professor in Electrical Engineering at HNU. His current research interests include AC/DC energy conversion systems, the analysis and control of power quality, as well as HVDC and FACTS technologies.